Monatshefte für Chemie 135, 269–278 (2004)
DOI 10.1007/s00706-003-0071-8

Monatshefte für Chemie
Chemical Monthly
Printed in Austria

Precursor-Support Interactions in Silica-Supported Manganese Oxide Catalysts

Ahmed K. H. Nohman*

Chemistry Department, Faculty of Science, Minia University, El-Minia 61519, Egypt

Received April 30, 2003; accepted (revised) June 5, 2003
Published online December 30, 2003

Summary. Catalyst materials investigated in this study were obtained by calcination of impregnated silica with $Mn(CH_3COO)_2 \cdot 4H_2O$ and $MnC_2O_4 \cdot 2H_2O$, so as to yield 10 wt% Mn/SiO_2. The precursor compounds as well as pure and impregnated silica support were calcined at 600 and 1000°C in a static air atmosphere for 5 h. Structural characteristics of the catalysts thus obtained were investigated by DTA, TG, XRD, IR and DRS. N_2 adsorption at −195°C was used for the assessment of surface texture of the test materials. Results of structural characterisation of catalysts obtained by calcination of manganese acetate-impregnated silica at 1000°C indicated the presence of strong silica-precursor interactions. Species of manganese silicates were detectable. Moreover, the decomposition of manganese acetate enhanced the transformation of amorphous silica into well crystallised α-quartz. In contrast, Mn_2O_3, Mn_3O_4, and minor proportions of MnO were detected in the catalysts derived from the manganese oxalate-impregnated silica. This has been ascribed to much weaker precursor/support interactions in the oxalate-impregnated silica than the acetate-impregnated one.

Keywords. Silica; Manganese acetate and oxalate; MnO_x; Interactions.

Introduction

Silica-supported manganese oxide catalysts are known of potential performance in oxidation processes: selective oxidation, total oxidation (combustion), and oxidative coupling reactions [1, 2]. Moreover, they are successfully used as oxygen-scavengers for ultrapurification of inert and olefinic gases to be used in oxygen sensitive catalytic reactions [3, 4]. These various oxygen treating activities are largely dependent on the surface structure of the Mn–O species, which in turn is controlled by the kind of synthetic events occurring at the precursor/support interfaces established during the preparation course of the MnO_x/silica catalysts.

Silica (SiO_2) is widely used as support material for a range of metal and metal oxide catalysts. This is considered to be owing to its high surface area, catalytic

* Corresponding author. E-mail: nohmana@yahoo.com

inertness, and high dispersing capability towards the loaded catalytic species [5, 6]. The supporting function of silica, and its contribution to the synthetic route of the supported catalyst, are closely related to acid-base properties and population of its surface hydroxyls (Si–OH), termed ''silanol groups'' [7]. In aqueous solutions the ionisation of free surface Si–OH groups can be schematically represented as follows:

(i) At $pH > pH_{zcp}$ (Scheme I)

$$\text{Si–OH} + \text{OH}^- \rightarrow \text{Si–O}^- + \text{H}_2\text{O}$$

$$\text{Si–O}^- + (\text{cation})^{n+} \rightarrow \text{Si–O(cation)}^{(n-1)+}$$

(ii) At $pH < pH_{zcp}$ (Scheme II)

$$\text{Si–OH} + \text{H}^+ \rightarrow \text{Si–OH}_2{}^+$$

$$\text{Si–OH}_2{}^+ + (\text{anion})^{n-} \rightarrow \text{Si–OH}_2{}^+(\text{anion})^{(n-1)-}$$

Where pH_{zcp} of silica (i.e., pH at zero-charge point of the surface) [7] occurs in the range $pH = 1$–2.

It is obvious that due to the very low pH_{zcp} of silica (very strong acidic regime) the surface adsorption selectivity is largely tilted towards cationic species from solutions of a wide range of acid–base properties ($pH > 2$). Accordingly, manganese nitrate has been widely used as a precursor compound in the preparation of silica-supported manganese oxide catalysts (for example Refs. [4, 5, 8, 9]). The expected strong adsorption of aqua-Mn^{2+} ions on silica has been found to be followed by strong interactions with the support surface at high temperature regimes, leading to high dispersion of the resulting Mn–O species [5, 8–11]. Some authors have even proposed formation of $MnSiO_x$-like surface species [1, 9, 11]. The MnO_x/SiO_2 interactions are intimately related to the preparation procedure, manganese content, and the calcination variables applied.

The present investigation was intended to explore the merits of using infrequently adopted precursor compounds; namely, manganese acetate and oxalate, in the preparation of MnO_x/SiO_2 catalysts. Moreover, the fact that manganese oxalate is less readily soluble in aqueous media than the acetate compound was meant to examine the role of solubility of the precursor on the surface structure of the final catalysts. Accordingly, the catalysts thus obtained were analysed for the surface structure and texture, as well as bulk properties.

Results and Discussion

Bulk Phase Composition

The thermal behaviours revealed by TG and DTA analyses for the uncalcined *AS* (acetate-impregnated silica) and *OS* (oxalate-impregnated silica) samples are exhibited in Fig. 1. The TG curve of *AS* exhibits two mass loss steps: (i) a gradual step ceasing near ~200°C with a mass loss of about 6%; and (ii) a steep one maximized at ~300°C leading to an additional mass loss of ~7%. Thereafter,

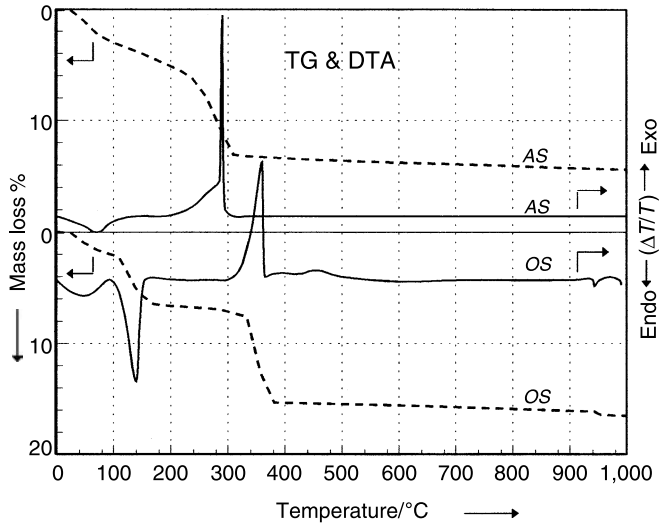

Fig. 1. TG and DTA obtained for *AS* and *OS* in flowing air ($20\,cm^3$/min) at a heating rate of 10°C/min

the material does not seem to suffer significant mass loss upon further heating up to 1000°C, making the total mass loss reach *ca.* 14.6%. The corresponding DTA curve (Fig. 1) shows the first mass loss step to be endothermic in nature, whereas the second is exothermic. Low-temperature, endothermic mass losses are usually ascribed to desorption of physisorbed molecules (mostly of water). On the other hand, the subsequent exothermic mass loss may be attributed to decomposition of the impregnated manganese acetate species.

The oxalate-impregnated silica (*OS*) also seems to decompose exothermally through the TG-observed mass loss step maximized at ~350°C, after being endothermally dehydrated through the mass loss step completed near 150°C (Fig. 1). The minor exotherm at 460°C, and the minor endotherm at ~950°C, are presumably owing to crystallization and/or oxidation of MnO_x species and the subsequent decomposition into Mn_3O_4, respectively [12 and Refs. therein]. These thermal events, though weak and ill-defined, are indicative of the initial decomposition of the impregnated oxalate precursor species into MnO_x-particles. Accordingly, in the case of *AS*, the absence of similar DTA-events following the decomposition of the acetate precursor species may be considered indicative of strong dispersion of the MnO_x species (*i.e.* strong precursor/support interactions). It is worth noting, that mass losses determined following isothermal calcination at 600 or 1000°C for 5 h (Table 1) are in fair agreement with those monitored by the non-isothermal TG measurements. This reveals that the calcination duration (5 h) has insignificant effect on mass loss magnitudes.

XRD powder diffractograms obtained for various test samples are shown in Fig. 2. It is obvious that the non-impregnated silica support (*S*) remains noncrystalline versus calcination at 600°C (*S*6) and 1000°C (*S*10). The corresponding calcination products of the unloaded manganese acetate (Fig. 2) and oxalate (not included) are shown to exhibit diffraction patterns very similar to those filed for

Table 1. Mass loss data

Sample	Mass loss %			
	Calcination		TG	
	600°C	1000°C	600°C	1000°C
S	–	–	4	6
A	64.7	65.8	65.0	65.0
AS	13.8	15.1	13.8	14.6
O	58.0	57.0	58.0	58.0
OS	15.8	15.8	15.0	16.5

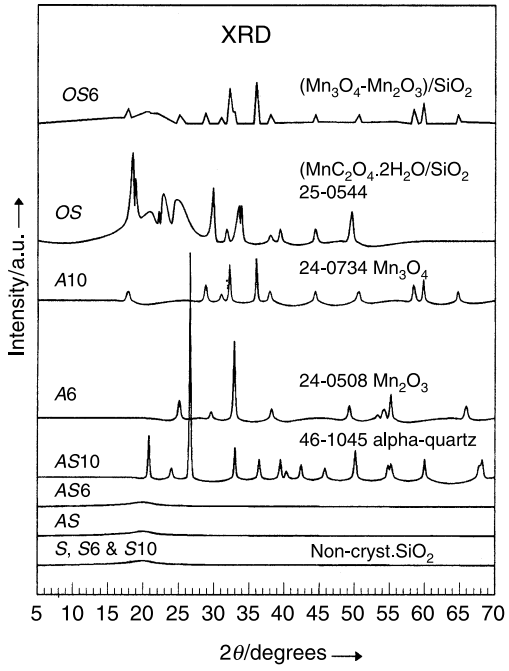

Fig. 2. X-Ray diffractograms obtained for the indicated samples

Mn_2O_3 (JCPDS 24-508) and Mn_3O_4 (JCPDS 24-734). The sole detectable difference between the crystalline phase compositions of the calcination products of the unloaded precursors lies in that of *A*6 as compared to *O*6. Whereas the former calcination product is composed solely of Mn_2O_3, the latter is shown to additionally contain an appreciable amount of Mn_3O_4. A similar result was observed previously and attributed to the reductive impacts of CO molecules only found in the volatile decomposition products of the oxalate compound [12].

When impregnated onto silica, acetate precursor species do not display any characteristic diffraction peaks in the diffractogram exhibited by *AS*, whereas *OS* is shown to display characteristic diffraction peaks of $MnC_2O_4 \cdot 2H_2O$ (JCPDS 25-544). These results are in line with the DTA results in suggesting much stronger

dispersive interactions at the acetate/silica than oxalate/silica interfaces. The strong interactions at the acetate/silica interfaces have been extended to the calcination products *AS*6 and *AS*10 (Fig. 2), where the former calcination product is shown to display nothing but the featureless XRD of the noncrystalline support, and the XRD of *AS*10 declares crystallization of the support into α-quartz as well as weak indications for formation of microcrystalline $MnSiO_x$ species. On the other hand, the weak interactions at the oxalate/silica interface have been reflected in the formation of XRD-detectable Mn_2O_3 and Mn_3O_4 particles upon calcination at 600°C. At 1000°C (*OS*10) the same oxide species were detected in addition to minor proportions of MnO particles. The sparingly soluble nature of manganese oxalate in water and, hence, formation of poor contact surfaces with silica is most probably the reason behind that behaviour.

Figure 3 comprises IR spectra obtained for the acetate-impregnated series of samples. All of the characteristic bands observed for unloaded manganese acetate are shown to disappear on supporting, except for the $\bar{\nu}(COO^-)$ bands (compare the spectra of *A* and *AS* at 1600 and 1400 cm^{-1} [13]). These results may imply that manganese acetate is, therefore, grafted on the silica surface as proposed in the following equation:

$$\underset{\text{(Support surface)}}{\text{Si–OH}} + \underset{\text{(Precursor in solution)}}{\text{Mn(OOC–CH}_3)_2} \xrightarrow{\text{Drying}} \underset{\text{(Grafted form)}}{\text{Si–O–Mn–OOC–CH}_3} + \text{CH}_3\text{COOH} \uparrow$$

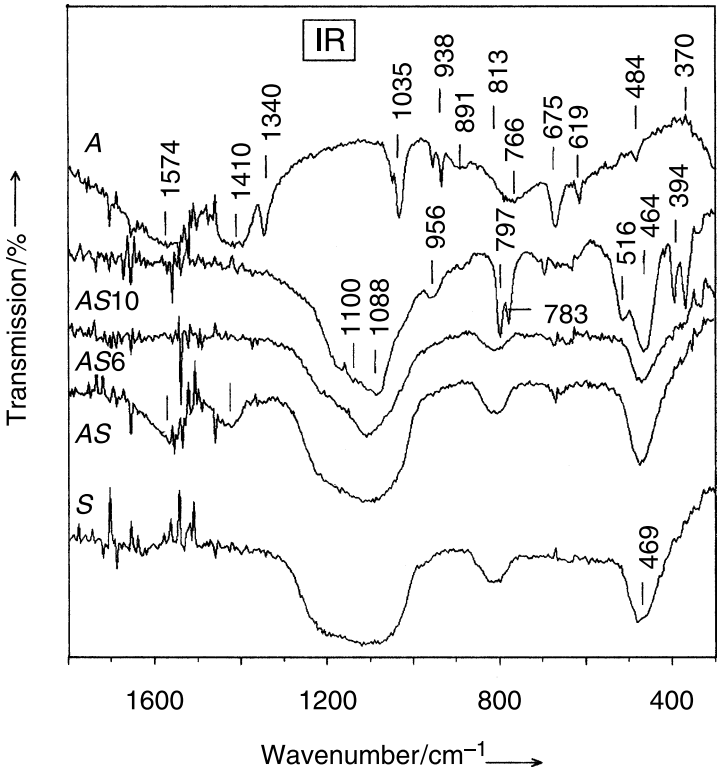

Fig. 3. IR spectra obtained for the indicated *AS* series of samples

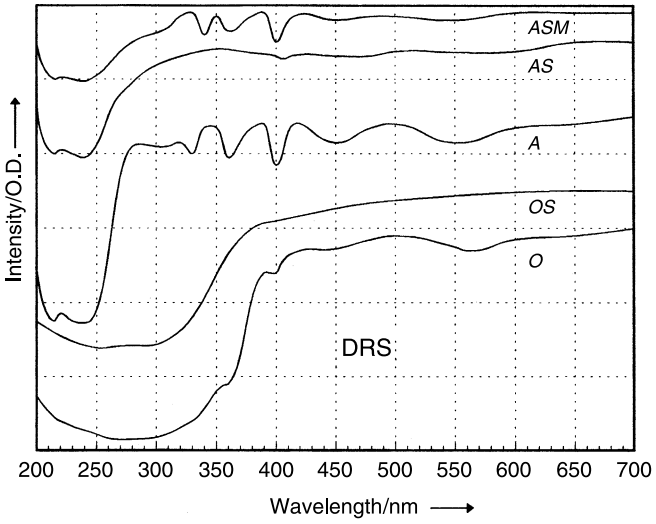

Fig. 4. DRS spectra obtained for *A*, *ASM*, *AS*, *O*, and *OS* samples (*ASM* = physical mixture of $A + S$)

This may owe its occurrence to the basic character of the impregnating acetate solution ($pH \sim 8$), which according to Scheme I would render the silica surface acquire a net negative charge. It is worth reporting that acetic acid was consistently smelt during the drying process. The DRS spectra (Fig. 4) of *A* and *AS* are not identical, thus revealing different coordination symmetries of Mn ions. This was also emphasised by taking a DRS spectrum of a physical mixture of manganese acetate and silica of the same proportions of *AS*; termed *ASM* in Fig. 4. The spectrum exhibited the same band structure of *A*. This may underline the occurrence of strong adsorptive interactions between the acetate impregnating solution and the silica support. It is, in fact, worthy indicating that the IR results sustain clearly the XRD findings regarding the quartz phase detected in *AS*10. The two IR band doublets at around 800 and 400 cm^{-1}, Fig. 3, are characteristic of α-quartz [14]. The IR spectra taken of *AS*6 and *AS*10 fail to monitor absorptions due to Mn–O vibrations of manganese oxide (MnO_x) species. Such absorptions (for example: at $\bar{\nu} \sim 615$, 575, 525, 510, and 350 cm^{-1}) were clearly observed in spectra taken of *A*6 and *A*10 (not shown).

In line with the XRD and DTA results, the IR findings for manganese oxalate on silica (spectra not shown) revealed the presence of precursor particles on silica. It is also to be noted, that the α-quartz phase was not detected in case of *OS*10. Thus, the crystallisation of silica into α-quartz is probably enhanced by highly dispersed Mn^{II} ions originating from the acetate decomposition rather than from the oxalate.

Furthermore, IR spectra (Fig. 3) obtained for pure silica (*S*) and the uncalcined and calcined *AS* samples display broad bands around $\bar{\nu} = 1100$, 800, and 500 cm^{-1}. These bands are characteristic of siloxane groups (Si–O–Si) [7]. Such Si–O–Si bridges are presumably formed upon condensation of two silanol groups at high temperatures:

$$2\ \text{Si–OH} \rightarrow \text{Si–O–Si} + H_2O$$

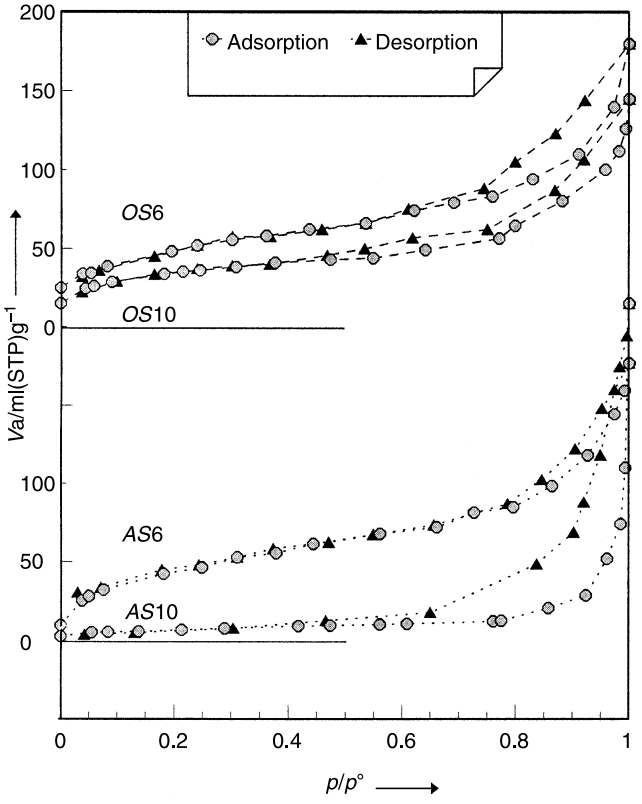

Fig. 5. N_2 adsorption isotherms measured at −195°C for *AS*6, *AS*10, *OS*6, and *OS*10

This, however, doesn't necessarily mean that all silanols are converted into siloxane groups; it is rather a part of these silanols that undergoes this transformation.

Surface Texture

N_2 adsorption has been employed to probe the catalysts' textural properties with the view of relating it to the apparent bulk characteristics discussed in the previous section. Fig. 5 exhibits the adsorption–desorption isotherms of the supported catalyst samples (*AS*6, *AS*10, *OS*6, and *OS*10). According to the IUPAC classification [15], the isotherms are generally of type IV. Thus, they account for a mesoporous character, giving rise to type H3 hysteresis loops, *i.e.* the pores are slit shaped [15, 16]. The lower p/p° closure point of the hysteresis loops lies within the normal range $p/p^\circ \geq 0.42$ [16]. A BET-analysis of the adsorption data resulted in the S_{BET} values given in Table 2. Inspection of the listed values reveals a loss of surface accessibility of silica upon loading MnO_x species. The decrease is more pronounced for the 1000°C calcination products, probably due to activation of particle sintering. In support, the porosity of the samples seem to be slightly altered on comparing the hysteresis loops of the isotherms for the samples calcined at 600 and 1000°C, which is more pronounced in the case of *AS*6 and *AS*10.

Table 2. Surface texture data

Sample	$S_{BET}/m^2\,g^{-1}$
S	200
*S*6	185
*S*10	170
A	–
*A*6	<5
*A*10	<5
O	–
*O*6	<5
*O*10	<5
uncertainity	±3

	$S_{BET}/m^2\,g^{-1}$	$V_{p(total)}/cm^3\,g^{-1}$ [a]	$r_p/Å$ [b]
AS	90	–	–
*AS*6	168	0.32	38
*AS*10	24	0.26	215
OS	142	–	–
*OS*6	160	0.27	34
*OS*10	132	0.22	16
uncertainity	±3	±0.02	±2

[a] $V_{p(total)}$: total pore volume; [b] r_p: pore radius $= 2V_{p(total)} \times 10^4/S_{BET}$

The values of total pore volume ($V_{p(total)}$) and pore radius (r_p) compiled in Table 2 also indicate diversity in pore dimensions. The different possible ways of linking together the (SiO_4) tetrahedra to give amorphous or ordered products of silica is, probably, responsible for the diversity of pore structure.

Moreover, Table 2 indicates that the 600°C calcination products (*AS*6 and *OS*6) exhibit maximal S_{BET} values amongst the supported catalyst samples. This may be interpreted in either of two ways, or both. The first is the probable generation of pores via evolved gaseous products of precursor decomposition [17]. The second is the opening of existing pores as a result of removal of trapped water and hydroxyls upon calcination at 600°C.

Conclusions

The above presented and discussed results may help drawing the following conclusions:

1. Surface texture and bulk characteristics of pure silica (amorphous character) are not markedly affected by thermal treatment. These properties are however affected after modification with MnO_x species.
2. MnO_x-induced modification of silica depends largely on the strength of adsorptive and dispersing interactions occurring respectively at the liquid/solid and solid/solid interfaces established during the preparation course of the MnO_x/SiO_2 catalyst samples.

3. The strong interactions established at the acetate/silica interfaces facilitate monolayer sort of dispersion of the resulting MnO_x species at 600°C, and crystallization of silica into α-quartz at 1000°C.
4. The weak interactions established at the oxalate/silica interfaces lead to formation of XRD-detectable particles of Mn_2O_3, Mn_3O_4, and MnO at 600°C, which are largely converted into Mn_3O_4 at 1000°C.

Experimental

Catalyst Preparation

The silica support, Degussa Aerosil-200 ($200\,m^2/g$), denoted "*S*", was calcined at 600 and 1000°C (for 5 h) in a static atmosphere of air. The calcination products are designated *S*6 and *S*10, respectively.

Manganese acetate [$Mn(CH_3COO)_2 \cdot 4H_2O$, 99.9% pure product of Strem, designated "*A*"] and oxalate [$Mn(C_2O_4) \cdot 2H_2O$, 99.9% pure product of Strem, designated "*O*"] were used to prepare aqueous impregnating solutions with concentrations leading eventually to 10 wt % Mn in the final catalysts. They were loaded onto the silica support by wet impregnation, vacuum drying at 50°C and $\sim 10^4$ Pa (for 24 h), and calcination at 600 or 1000°C for 5 h. Portions of the unsupported precursors were similarly calcinated at 600 or 1000°C for 5 h. The calcination products (*i.e.* the catalysts) of the supported and unsupported precursors are designated similarly to those of the support. Hence, *A*6 indicates the 600°C-calcination product of unsupported manganese acetate, whereas *OS*10 signifies the 1000°C-calcination product of manganese oxalate-impregnated silica.

Catalyst Characterisation

Thermal analyses (TG and DTA) were carried out in a static atmosphere of air by means of a DT-30H Shimadzu thermal analyzer (Japan). Small portions (10–25 mg) were used of the test samples, and α-Al_2O_3 (Shimadzu Corp.) was the thermally inert material used for the DTA measurements. X-Ray powder diffractometry (XRD) was performed by means of a model JSX-60 PA Jeol diffractometer (Japan) equipped with Ni-filtered Cuk_α radiation ($\lambda = 1.5418$ Å) and operated at 40 kV and 30 mA. For infrared spectroscopy, IR spectra were taken of wafers of lightly loaded (≤ 1 wt%) KBr-supported samples in the spectral range $\bar{\nu} = 4000-200\,cm^{-1}$ and at a resolution of $4.3\,cm^{-1}$, using a model 580B Perkin-Elmer spectrophotometer (UK). On the other hand, UV-Vis diffuse reflectance spectroscopy (DRS) was carried out employing a model UV-2100 UV-visible automatically recording Shimadzu spectrophotometer (Japan), equipped with a reflectance attachment. The spectra were recorded in the wavelength range $\lambda = 900-200$ nm. N_2 adsorption–desorption isotherms at -195°C were determined volumetrically, using a home-made all-Pyrex glass microapparatus similar to the design described elsewhere [16]. Test samples were outgassed at ~ 140°C (for 3 h) and $1.33 \cdot 10^{-7}$ Pa prior to exposure to the nitrogen atmosphere. Following IUPAC recommendations [15, 18], the adsorption data were processed using the mathematical apparatus of the BET model [16] for the specific surface area ($S_{BET}/m^2\,g^{-1}$) and *Kelvin* model [16] for pore volume calculations [16].

References

[1] Sofranko JA, Leonard JJ, Jones CA (1987) J Catal **103**: 302
[2] Jones CA, Leonard JJ, Sofranko JA (1987) J Catal **103**: 311
[3] Horvath B, Moeseller R, Horvath EG, Krauss HL (1975) Z Anorg Allg Chem **418**: 1
[4] Moeseller R, Horvath B, Lindenau D, Horvath EG, Krauss HL (1976) Z Naturforsch **31b**: 892
[5] Dollimore D, Pearce J (1980) Powder Technology **25**: 71

[6] Glinski M, Kijenski J, Jakubowski A (1995) Appl Catal A General **128**: 209
[7] Legrand AP (1998) The Surface Properties of Silicas. John Wiley, Chichester
[8] Horvath B, Strutz J, Moseler R, Horvath EG (1979) Z Anorg Allg Chem **449**: 5
[9] Zaki MI, Nohman AKH, Hussein GAM, Nashed YE (1995) Colloids and Surfaces A. Phys Chem Eng Asp **99**: 247
[10] Pott G, McNicol D (1971) J Discussions of the Faraday Society **57**: 121
[11] Vorobev VN, Nivarov VN, Razikov KKh (1985) Zh Obshch Khim **55**: 1913
[12] Zaki MI, Nohman AKH, Kappenstein C, Wahdan TM (1995) J Mater Chem **5**: 1081
[13] Nakamoto K (1997) Infrared and Raman Spectra of Inorganic and Coordination Compounds. Wiley, New York
[14] Gadsden GA (1975) Infrared Spectra of Minerals and Related Inorganic Compounds. Butterworths, London
[15] Sing KSW, Everett DH, Hall RAW, Moscou L, Pierotti RA, Rouquerol J, Siemieniewska T (1985) Pure Appl Chem **57**: 603
[16] Gregg SJ, Sing KSW (1982) Adsorption, Surface Area and Porosity, 2nd edn. Academic Press, London
[17] Nohman AKH, Ismail HM (1998) Colloids and Surfaces A. Phys Chem Eng Asp **136**: 237
[18] Everett DH, Parfitt GD, Sing KSW, Willson R (1974) J Appl Chem Biotechnol **24**: 199